Experiments on radiative collapse in laser-produced plasmas relevant to astrophysical jets

K. Shigemori,[1,2] R. Kodama,[1] D. R. Farley,[2] T. Koase,[1] K. G. Estabrook,[2] B. A. Remington,[2] D. D. Ryutov,[2] Y. Ochi,[1] H. Azechi,[1] J. Stone,[3] and N. Turner[3]

[1]*Institute of Laser Engineering, Osaka University, Suita, Osaka, 565-0871, Japan*

[2]*Lawrence Livermore National Laboratory, P.O. Box 808, Livermore, California 94551*

[3]*Department of Astronomy, University of Maryland, College Park, Maryland 20742*

(Received 16 May 2000)

We report a laser experiment of astrophysical interest on radiative jet formation. Conically shaped targets are irradiated by intense laser light. An ablated plasma flow collides at the axis of the cone targets, then propagates at high Mach number, forming a jetlike structure. We measure time-resolved x-ray self-emission images from the jets. The diameter of the jet increases with decreasing atomic number of the irradiated target, suggesting that the collimation is due to radiative cooling. Two-dimensional simulations reproduce essential features of the experimental results.

PACS number(s): 52.50.Jm, 52.35.Tc, 52.70.La, 98.38.Fs

Astrophysical jets are one of the most exciting phenomena in our universe. Previous observations provided well-collimated jet images ejected from active galactic nuclei [1] and from young stellar objects [2–4]. Protostellar jets such as (Harbig-Haro)-47 [2,4] were been well studied observationally [5–7]. They propagate at a high Mach number $M > 10$, and are well collimated and narrow. The reason for the significant collimation of these jets is not completely understood, but some calculations indicate that radiative cooling is a probable candidate for the collimation [8,9]. Radiative cooling is very important not only for the formation of radiative jets, but also in magnetic confinement fusion plasmas [10], *Z*-pinch plasmas [11], and laser-produced plasmas [12,13]. A recent experimental study indicated that a high-power laser allows the creation of a high Mach number radiative jet in the laboratory [14].

Motivated by astrophysical interest in radiative jets, in this Brief Report we focus on a study of radiation effects on the formation of high Mach number jets. Conically shaped targets were irradiated by a short burst of intense laser irradiation, and we measured the x-ray emission from the jet propagating from the target. Radiative effects are a strong function of the atomic number (Z). In order to isolate the effects of radiation in our laboratory jets under otherwise similar conditions, we varied the Z of the targets, employing CH (palyrene), Al, Fe, and Au. The higher-Z jets were narrow and collimated (''collapsed''), whereas the lower-Z plasma jets were much broader. We simulated the jet formation with the two-dimensional (2D) radiation-hydrodynamics code LASNEX [15]. The radiative cooling effect observed in the experimental results was reproduced by the 2D simulations, showing that radiative collapse occurs in the high-Z jets, but not in low-Z jets.

The experimental configuration is shown in Fig. 1. Conically shaped solid targets were irradiated by six beams of the frequency-doubled (wavelength 0.53 μm) GEKKO-XII Nd:glass laser [16] at the Institute of Laser Engineering, Osaka University. The full width at half maximum (FWHM) pulse duration of the laser and the total laser energy were 100 ps (Gaussian) and $\approx$500 J, respectively. The opening angle of the conically shaped target was 120°. The diameter of the cone targets was 1.6 mm. Five beams of the GEKKO laser irradiated the inner side of the cone target in a symmetric pentagonal orientation. The incident angle of each beam was 37.4° to the normal of the cone surface. An additional beam irradiated the center of the cone from the direction exactly face on to the cone target. We employed random phase plates [17] on all laser beams to generate an overall spatially uniform irradiation. The overlapped laser spot diameter and effective laser intensity were approximately 1.2 mm (FWHM) and $\approx 3\times 10^{14}$ W/cm^2, respectively.

When a high-intensity laser pulse irradiates a material, laser energy is absorbed, and the surface of the target is heated up. The heated mass is ablated from the surface as hot plasma, which moves rapidly away from the surface in a perpendicular direction. The ablated hot plasma ''implodes'' onto the axis of the cone. The axial component of the imploding plasma is largely unaffected, and the plasma ''jet'' propagates along the cone axis. In our estimation from the simulation (which is described later), the ion mean free path of the colliding plasma is very small even for the low-Z CH plasma; the ''interpenetration'' of the imploding plasma is negligible in this experimental condition. As the ablated plasma stagnates on the axis of the cone, the radial component of incoming momentum flux ($\rho_a v_s^2$) is converted to pressure on axis [$(Z+1)n_{jet}T_{jet}$]. Equating, and replacing ion number density with mass density, we have $\rho_a v_s^2$

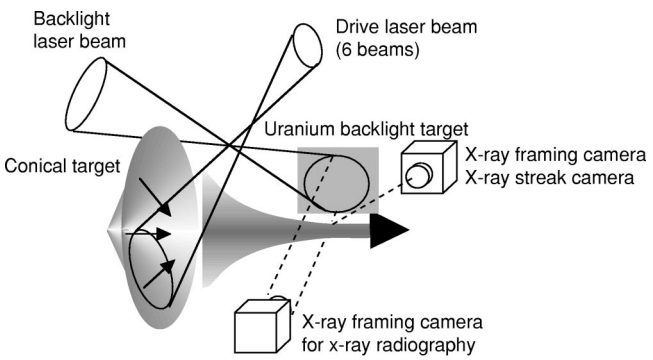

FIG. 1. Schematic view of the experimental setup.

 ©2000 The American Physical Society

$=\text{const}\times[(Z+1)/A]\rho_{\text{jet}}T_{\text{jet}}$, that is, $\rho_a v_s^2 \propto \rho_{\text{jet}}T_{\text{jet}}$. Hence, if radiation cools the plasma jet on axis, lowering the temperature, the density has to increase to maintain the pressure, an effect we call ''radiative collapse.'' Note, that the ablated plasma should emerge like a ''bullet'' [18], not a continuous outflow, because the pulse duration of the laser is relatively short. As we stated above, the formation of a well-collimated jet depends on radiative cooling. Since the radiation from the jet plasma increases with increasing ionization state ($\overline{Z}$) of the plasma, we employed four kinds of target materials: palyrene (C_8H_8: $Z=3.5$), aluminum (Al: $Z=13$), iron (Fe: $Z=26$), and gold (Au: $Z=79$).

We measured the x-ray self-emission from the jets. An x-ray framing camera (XFC) was used to obtain snapshots of two-dimensional self-emission images of the jets every 100 ps for 500 ps. The XFC was located at 90° to the axis of the cone target in order to have a side-on view of the jet. The XFC was coupled with a 15-μm-diameter pinhole imager with a magnification of 6. The temporal resolution and the spatial resolution of the XFC were 80 ps and 15 μm, respectively. Another XFC was also located at 90° to the axis of the cone, from but on the other side to observe a backlit image of the irradiated cone target by x-ray radiography. The uranium (U) backlight disk was located at 3 mm away from the axis of the cone target. The uranium backlighter target was irradiated by one beam of the GEKKO to generate a soft x-ray source. The pulse width, focusing diameter, and laser energy of the backlighter beam were 100 ps, 1.5 mm, and 80 J, respectively. The uranium backlighter emits x rays with the photon energy of around 1.0 keV [19]. We also measured the jet speed with an x-ray streak camera (XSC), which was located at 90° to the normal of the cone. The XSC is coupled to a 10×50-μm^2 slit imager with a magnification of 7. The temporal resolution and the spatial resolution of the XSC were 90 ps and 20 μm, respectively. The XSC measured the x-ray emission on the axis of the cone target. Data from the XFC's and the XSC were recorded onto charge coupled devise cameras.

Figure 2 shows the snapshots of two-dimensional self-emission x-ray images from the XFC for (a) CH, (b) Al, (c) Fe, and (d) Au target at 1.3 ns after the laser irradiation. The data show jetlike emission structures from the center of the cone. We can see the difference in the diameter of the x-ray emission between each jet, that is, the diameter increases with decreasing atomic number of the target. From the XSC image of the Au jet (not shown here), the peak intensity of the emission moves rapidly away from the cone target. This indicates that the high density mass from the cone target propagates rapidly like a bullet because the x-ray emission for optically thin plasma is a strong function of the ion density ($\sim n_i^2$), that is, the peak in emission coincides with the peak in density. The jet tip velocity was taken to be the velocity of the position of half maximum of the self-emission. The typical tip velocities were $(6-8)\times 10^7$ cm/s. The backlit radiograph Fe jet (at 2.0 ns) is shown in Fig. 2(e). We confirmed that the mass actually exists along the axis line of the cone from the snapshots of the backlit image. In our jets, we did not see any turbulence or knots caused by hydrodynamic or radiative hydrodynamic instabilities [20]. Note that the spatial resolution of the XFC

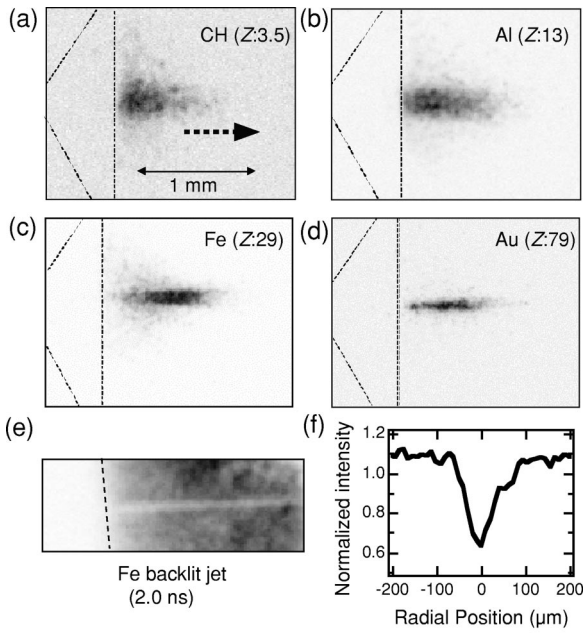

FIG. 2. Snapshots of two-dimensional side-on self-emission images from the XFC for (a) CH, (b) Al, (c) Fe, and (d) Au targets at 1.3 ns after the laser irradiation. (e) Backlit Fe jet image from the XFC at 2.0 ns, and (f) radial lineout plot at 1 mm from the center of the cone target.

is 20 μm, so features or perturbations smaller than this are not visible for our diagnostics in this experiment.

We analyzed the diameter of the jets for each spatial position, and each observation time from the two-dimensional self-emission images taken from the XFC. First, we plotted the peak intensity point for each image in order to determine the ''jet peak,'' because the peak intensity coincides with the peak density as describe above. Normalized lateral lineouts for the axial position corresponding to the location of peak intensity at 1.3 ns are shown in Fig. 3(a). We show this with

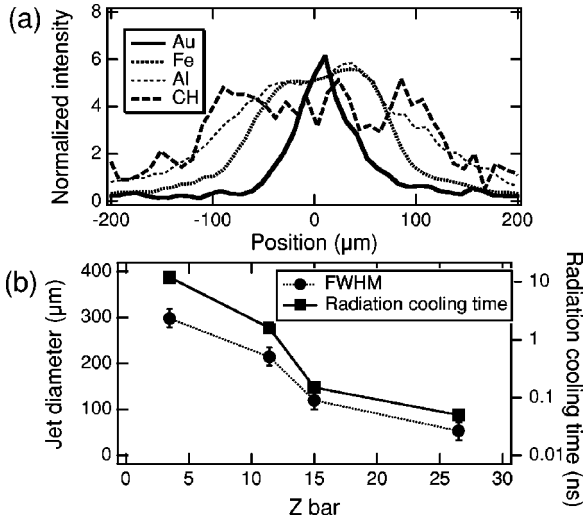

FIG. 3. (a) Lineouts of the four jets at 1.3 ns after the laser irradiation and at around the peak emission point of each jet. (b) Jet diameter and radiation cooling time vs effective ionization state $\langle Z\rangle$ for each jet. The radiation cooling time τ_{rad} and $\langle Z\rangle$ were calculated by the LASNEX 2D simulation.

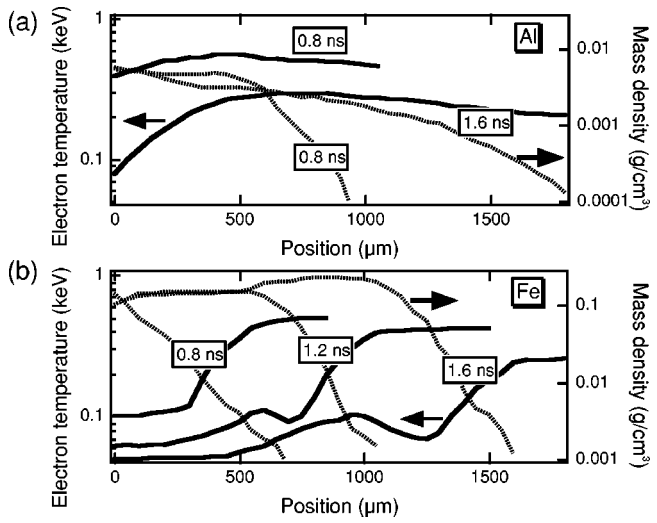

FIG. 4. Examples of the LASNEX 2D simulation of the (a) Al and (b) Fe jets. The solid curves and the dotted curves represent the electron temperature and the mass density in the jet propagation direction, respectively.

a plot of the diameter (FWHM) of each jet vs ionization state $\overline{Z}$ in Fig. 3(b). $\overline{Z}$ is calculated value from the LASNEX simulation for each target material. The radiation transport algorithm used in the simulations was multigroup diffusion assuming a non-local thermodynamic equilibrium plasma, with 256 to 512 bins encompassing photon energies from 1 eV to 30 keV and with detailed emission and absorption lines. It is very clear that the diameter of the self-emission decreases monotonically with increasing atomic number of the target. When the strong radiative cooling occurs, the density rapidly increases while the temperature drops to maintain pressure. Since the local sound speed of the plasma is determined by the temperature $[c_s=(\gamma P/\rho)^{1/2}\propto T^{1/2}]$, the sound speed decreases with radiative cooling. Since the radial flow velocity of the jet is approximately determined by the sound speed, the radiative collapse reduces the diameter of the jets, and slows any subsequent expansion.

Examples of the output from the LASNEX 2D simulations are shown in Fig. 4. Figure 4(a) gives electron temperature and mass density of the Al jet at several time steps, and Fig. 4(b) shows the same for Fe. The results shown represent the average from 10 to 30 μm from the axis of the cone. The dotted curves and the solid curves in the Fig. 4 represent the mass density and the electron temperature, respectively. The electron temperature of the Fe jet shows significant cooling in vicinity of the tip of the jet, while the electron temperature of the Al jet shows no evidence of cooling near the tip. Also, the mass density of the Fe jet increases with decreasing electron temperature around the tip of the jet. Note that the mass density of the Fe jet is higher than that of the Al jet by a factor of 50 at 1.6 ns, and at 1 mm. Although we observed backlit images for the higher-Z jets (Fe and Au), we were unable to record backlit images for the lower-Z jets (CH and Al), due to their lower overall optical depth. We can see weak radiative cooling of the Al jet at 1.6 ns near the cone target. However, the radiative cooling does not catch up with the jet propagation, resulting in formation of the ''adiabatic'' jet during our observation time scale. Thus the radiative collapse should be sensitive to the ratio of the radiative cooling time and the hydrodynamic time. We also did the calculation turning off the radiation transport (not shown here). The radiation-off calculation of high-Z jets resembles the adiabatic jets, that is, there is no obvious cooling during the jet propagation.

TABLE I. The dimensionless parameters (M: Mach number; χ: radiation cooling parameter) in our experiment and the Harbig-Haro (HH) jets.

Parameters	HH jets	CH jet	Au jet
M	10–20	2–8	10–50
χ	0.1–10	≈ 40	≈ 0.7

Since the criterion of the radiative jet should be determined by the ratio of the radiative cooling time to the hydrodynamic time, we calculated the radiation cooling time for all the jets using the LASNEX 2D simulations. The squares in Fig. 3(b) are the radiative cooling time $\tau_{\rm rad}$, which is defined as the plasma energy content divided by the radiative flux: $\tau_{\rm rad}=3n_e k(T_i/\overline{Z}+T_e)/2/q_{\rm rad}$, where n_e is the electron density, k is the Boltzman constant, T_i is the ion temperature, T_e is the electron temperature, and $q_{\rm rad}$ is the radiative flux. $\tau_{\rm rad}$ is from calculated values at 1.3 ns and at around the peak point of the self-emission. All the parameters were calculated by the LASNEX 2D simulation. This plot clearly shows that the radiation cooling time decreases with increasing $\overline{Z}$. The radiation cooling time of the Fe and Au jets is much smaller than a hydrodynamic time scale ($\tau_{\rm hydro}=R_{\rm jet}/c_s$), while for Al $\tau_{\rm hydro}<\tau_{\rm rad}$, and for CH, we have $\tau_{\rm hydro}\ll\tau_{\rm rad}$. This is consistent with our interpretation that the radiative collapse forms the well-collimated jets.

The radiation time scale can also be roughly estimated by a steady-state coronal equilibrium model [21]. This model assumes that the plasma is transparent to its radiation (optically thin), and that the electron collisional ionization rate is exactly balanced by the total recombination rate. The cooling rate q [erg/(cm^3 s)] is given by $q=n_e n_i\Gamma=\overline{Z}n_i^2\Gamma$, where the ''cooling curve'' $\Gamma(T_e)$ is given graphically in reference [21] as erg cm^3/s. For Fe at $T_e=0.5$–1.0 keV, this model gives $\Gamma=5\times10^{-19}$ erg cm^3/s$=3\times10^{-7}$ eV cm^3/s. Dividing the plasma energy content by the cooling rate, we write the radiation cooling time ($\tau_{\rm rad}$) as $\tau_{\rm rad}=[(3/2)(\overline{Z}+1)n_iT]/(\Gamma\overline{Z}n_i^2)\approx 5\times10^6 T$ (eV)$/n_i$, since $\overline{Z}$ is relatively large ($\approx$15 both from the LASNEX simulation and from Ref. [21]. Since the radiation cooling time is approximated as $\tau_{\rm rad}\sim 1/n_i\sim 1/\rho$, if $\rho=10^{-2}$ g/cm^3, then $\tau_{\rm rad}\approx 50$ ps, or if $\rho=5\times10^{-3}$ g/cm^3, which is the result from the simulations $\tau_{\rm rad}\approx 100$ ps. This estimate suggests that the radiative cooling occurs in the early moments ($t<\sim 1$ ns) in our experiment. Note also that the cooling parameter for Al at $T_e=0.5$–1.0 keV given in Ref. [21] is $\sim 2\times10^{-20}$ erg cm^3/s, i.e., a factor of 25 smaller than that of Fe and at the same temperature. This is consistent with our observation that the Al is not radiatively cooled, whereas the Fe is.

In Table I, we compare some important dimensionless parameters in our laser-produced jets with those in the astrophysical jets. The ranges of the dimensionless parameters for typical astrophysical jets are taken from Refs. [8,9]. The pa-

rameters for the laboratory jets are taken from LASNEX 2D simulations. An important dimensionless parameter of the hydrodynamics of jets is internal Mach number $M = v_{\rm jet}/c_s$, the ratio of velocity of the jet $v_{\rm jet}$ to the sound speed c_s within the jet. We confirmed that the jet velocity $v_{\rm jet}$ for each target material shows good agreement with that from LASNEX simulation. Also compared is the dimensionless radiative cooling parameter χ, which is the ratio of the cooling length to the radius of the jet $(v_{\rm jet} \cdot \tau_{\rm rad}/R_0)$, where R_0 is the radius of the jet at the location of peak self-emission. When χ is small, $\chi < 1$, the jet is ''radiative'' because the radiation cooling time is smaller than the hydrodynamic time. We used calculated values from the LASNEX simulation except for R_0. The χ in Table I are values at 1.3 ns and at the jet peak. The Mach number M of our jets is very close to that of the astrophysical jets. Since the sound speed of the high-Z jet is reduced by the radiative cooling, the Mach numbers of the high-Z jets are relatively higher than those of the low-Z jets. The ratio of the jet density to ambient medium η is much larger than that of the astrophysical jets, because our experiments were conducted at nearly vacuum ($\rho_{\rm amb} \approx 10^{-11}$ g/cm^3). On the other hand, the radiative cooling parameter χ is of the same order of magnitude as astrophysical jets. The χ values for our laboratory jets differ by up to a factor of 50 between Au and CH, showing that we span nearly adiabatic to radiatively cooled conditions.

In conclusion, we have developed laboratory jet experiments relevant to astrophysical jets. The experimental results show that jets of high-Z material are more radiatively cooled and are well collimated, whereas low-Z materials jet are adiabatically expanded. The experimental results were well reproduced by 2D LASNEX simulations. The simulation results indicates that the radiative cooling time is important for the formation of the well-collimated jets. The internal Mach numbers and radiative cooling parameters of our experimental jets are relevant to those of the astrophysical jets.

The authors acknowledge the staff at the Institute of Laser Engineering, Osaka University. This work was performed in part under the auspices of the U.S. DOE by the Lawrence Livermore National Laboratory under Contract No. W-7405-ENG-48, and supported in part by the LLNL LDRD, Grant No. 98-ERD-022.

[1] A.H. Bride *et al.*, Annu. Rev. Astron. Astrophys. **22**, 319 (1984).
[2] R. Schwartz, Astrophys. J. **212**, L25 (1977).
[3] M.A. Dopita *et al.*, Astrophys. J. **263**, L73 (1982).
[4] H. Zinnecker *et al.*, Nature (London) **394**, 862 (1998).
[5] B. Reipurth and S. Heathcote, Astron. Astrophys. **246**, 511 (1991).
[6] B. Mundt, Can. J. Phys. **64**, 407 (1986).
[7] S. Heathcote *et al.*, Astrophys. J. **112**, 1141 (1996).
[8] J.M. Blondin *et al.*, Astrophys. J. **360**, 370 (1990).
[9] J.M. Stone and M.L. Norman, Astrophys. J. **413**, 198 (1993).
[10] E. Bitter *et al.*, Phys. Rev. Lett. **71**, 1007 (1993).
[11] J.W. Shearer, Phys. Fluids **19**, 1426 (1976).
[12] E.F. Gabl *et al.*, Phys. Rev. Lett. **63**, 2737 (1989).
[13] L.J. Dhareshwar, Phys. Fluids B **4**, 1635 (1992).
[14] D.R. Farley *et al.*, Phys. Rev. Lett. **83**, 1982 (1999).
[15] G.B. Zimmerman and W.L. Kruer, Comments Plasma Phys. Control. Fusion **2**, 51 (1975).
[16] C. Yamanaka, IEEE J. Quantum Electron. **QE-17**, 1639 (1981).
[17] Y. Kato *et al.*, Phys. Rev. Lett. **53**, 1057 (1984).
[18] J.M. Stone *et al.*, Nature (London) **377**, 315 (1995).
[19] S.G. Glendinning *et al.*, Proc. SPIE **2523**, 29 (1995).
[20] R. Ouyed *et al.*, Nature (London) **385**, 409 (1997).
[21] D.E. Post *et al.*, At. Data Nucl. Data Tables **20**, 397 (1977).